Transition metals-early transition alloys and (2) Transition metal-rich and metalloid alloys (produced by Hitachi Metals Ltd., Vacuumschmelze GmbH & Co. KG and in our laboratory by electrochemical deposition methods). Early transitions metals (such as Sc) and metalloids (such as P, B, and Si) are known as glass forming element.

All the metallic glasses studied by us - except of amorphous $Ni_{86}P_{14}$ and $Co_{80}P_{20}$ alloys - were prepared by melt spinning. The preparation of $Ni_{90}Sc_{10}$, $Co_{90}Sc_{10}$ and $Fe_{90}Sc_{10}$ alloys was performed in a high vacuum chamber. The amorphous $Ni_{86}P_{14}$ and $Co_{80}P_{20}$ alloys were prepared by the electrochemical deposition methods [23,24].

The atomic structures of the metallic glass were studied using high-energy XRD (HE-XRD) with a photon wavelength of 0.21 Å at the beamline BL04B2 at SPring-8. The beamline BL04B2 is designed for diffraction and scattering experiments at photon energies larger than 37 keV. The main advantage of the beamline is the ability to structurally characterize disordered samples by employing a wide range of scattering vectors *Q* and a low instrumental background. Further advantages are small correction terms (especially for absorption correction) and reduction of truncation errors. The analysis of High-Energy X-Ray Diffraction (HE-XRD) data and the transformation from k space to the real space is described elsewhere [18].

Results

Figure 1 shows the radial distribution function of crystalline bcc-Fe, fcc-Ni and hcp-Co and of the amorphous transition metal-rich $Fe_{90}Sc_{10}$ alloy. As may be seen with the similarity exists between pattern of the peaks of the RDF of amorphous $Fe_{90}Sc_{10}$ alloy and crystalline Fe with a bcc structure. However, the peaks of the amorphous alloy (Figure 1) are broader than the ones of the Fe bcc crystals and the positions of the peaks are shifted which indicates different interatomic spacing in the amorphous $Fe_{90}Sc_{10}$ alloy and crystalline Fe. The similarity between pattern of the peaks of the RDF of amorphous $Fe_{90}Sc_{10}$ alloy and crystalline Fe with a bcc structure indicates that the atomic structure of the amorphous alloy can be described as arrangements of distorted cluster with a bcc structure (the peaks of the amorphous alloy were broader than the ones of the Fe bcc crystals) and a distribution of interatomic spacing centered on those of bcc-Fe with a certain shift of the peak positions. In pure bcc-Fe, the nearest neighbor (nn) and the next nearest neighbor (nnn) atoms are located at 2.48 Å and 2.87 Å, respectively, with 8 atoms and 6 atoms as nn and nnn in the corresponding distances. Due to the small difference between the nn and nnn shells in bcc-Fe, the nn and nnn shells overlap in the amorphous alloy so that the nn and nnn shells become - in amorphous metal-rich alloy - indistinguishable.

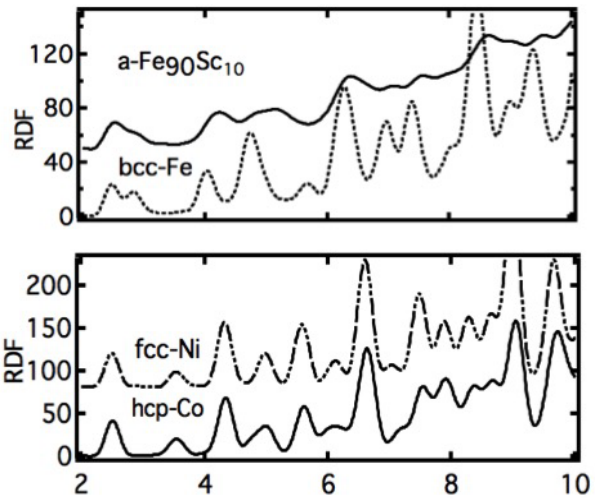

Figure 1: RDF of crystalline hcp-Co, fcc-Ni. bcc-Fe, and amorphous $Fe_{90}Sc_{10}$ alloy. The values of RDF in y-axis are valid for bcc-Fe and hcp-Co. In order to see the different RDFs, the values for amorphous alloy and fcc-Ni are shifted with a constant.

As may be seen from Figures 2 and 3, the RDF's of crystalline bcc-Fe and the RDF's of amorphous $Co_{90}Sc_{10}$ and $Ni_{90}Sc_{10}$ alloys yields the same result as for $Fe_{90}Sc_{10}$ alloy. The following two main features of the peak pattern of all three alloys are as follows: (1) All the peak patterns of the RDFs are identical; (2) The major differences between them are the enhanced peak widths and the shifts of peaks of the individual amorphous metal-rich alloys relative to the peaks of the bcc-Fe. In other words, the SRO and MRO of metal-rich alloys can be described to consist of chemically disordered and structurally distorted clusters with a bcc atomic arrangement. Figure 4 shows a schematic drawing of two-dimensional atomic arrangements of the nn and the nnn in a bcc cluster and the corresponding arrangements in a distorted bcc cluster with a Sc-atom in the center. Because of the different electronegativity of Fe and Sc, the Sc-atoms have the tendency to attract the Fe- atoms.

On the other hand, it may be noted that according to the results reported above, the bcc clusters making up the amorphous structures seem not to be correlated with the crystal structure of main transition metal, i.e., bcc for Fe, fcc for Ni and hcp for Co.

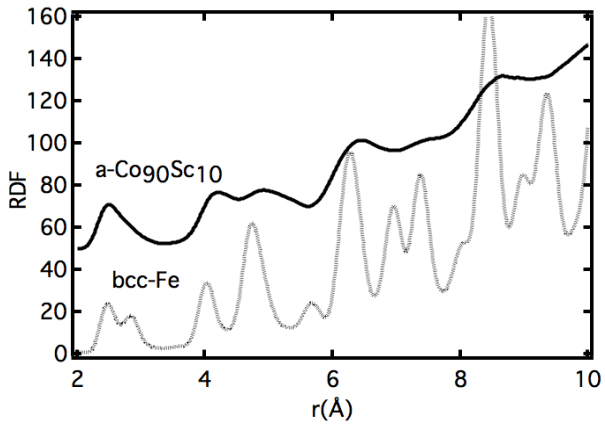

Figure 2: RDF of crystalline bcc-Fe, and amorphous $Co_{90}Sc_{10}$ alloy.

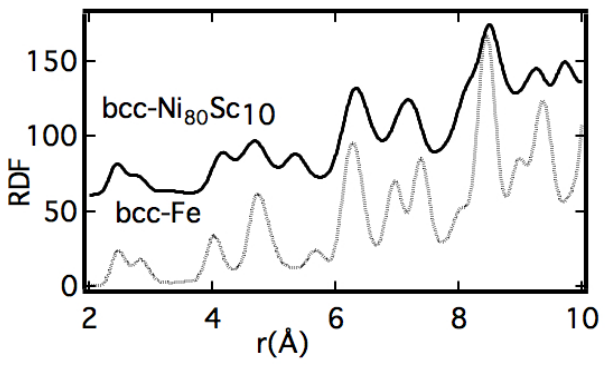

Figure 3: RDF of bcc-Fe and distorted bcc structure of crystalline $Ni_{90}Sc_{10}$ alloy with long-range order.

In summary, the similarities of the RDFs of amorphous transition metal-rich alloys of Fe, Ni and Co, indicate that the structure of all of these alloys consist of distorted bcc clusters. For amorphous alloys with transition metal compositions larger ≥ 78 at percentage, the structure seems independent of the second components of these alloys with such as Sc, B, Si or P as presented in Figure 5. Finally, let's address the question: Why are the distorted bcc clusters the preferred structural units of the amorphous metal–rich alloys. In order to discuss this question, the structure factor, S(Q), of amorphous $Fe_{90}Sc_{10}$ alloy as a function of $Q=4\Pi/\lambda$ was compared, Figure 6 [25] by means of the pair correlation functions with the S(Q) of molten Fe at T=1870 K and at 1830 K (the melting temperature of Fe is T_m=1811 K) and with the S(Q) of an undercooled melt of Fe at T=1750 K, 1730 K and 1670 K. As may be seen, the position of peaks in the S(Q) plots (up to about 1 Å) and the number of the nn are similar in the amorphous $Fe_{90}Sc_{10}$, in the melt and in the undercooled Fe melt. This experimental observation suggests that in rapidly quenched melts bcc clusters are the preferred structural units.

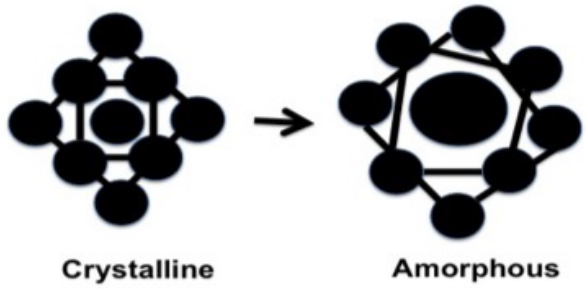

Figure 4: A two-dimensional bcc structure and a distorted bcc structure. The large and small black circle presents a Sc-atom and Fe- atoms respectively. The displacement of atoms in amorphous alloys from the fixed positions of bcc-Fe at the nn and nnn positions causes an overlap between nn and nnn.

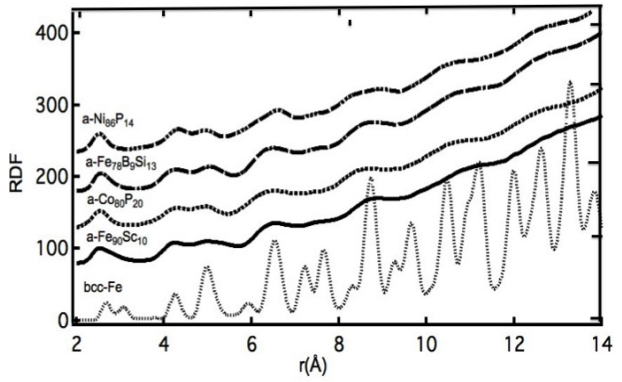

Figure 5: PRDF of bcc-Fe, and rapid quenched samples. The value of RDF of bcc-Fe in x-axis is about 0.3 Å shifted. This achieves the best agreements with amorphous metals. Above 14 Å, there are no correlations between atoms in amorphous state.

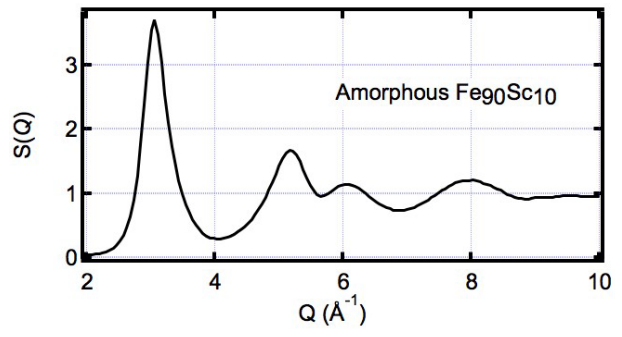

Figure 6: Structure factor S(Q) of amorphous $Fe_{90}Sc_{10}$ alloy as a function of $Q=4\Pi/\lambda$.

Acknowledgements

This work is supported by the National Natural Science Foundation of China (Grant no. 51571119, 51520105001), the Natural Science Foundation of Jiangsu Province and the Fundamental Research Funds for the Central Universities. T. F. acknowledges the support by the innovation project and the specially-appointed professor project of Jiangsu province. The synchrotron radiation experiment was approved by the Japan Synchrotron Radiation Research Institute (proposal. 2015A1890).

References

1. Wu ZW, Li MZ, Wang WH, Liu KX (2015) Hidden topological order and its correlation with glass-forming ability in metallic glasses. Nat Commun 6: 6035.
2. Polk DE (1970) Structural model for amorphous metallic alloys. Scripta Met 4: 117-122.
3. Cargill GS (1970) Structural investigation of noncrystalline Nickel-Phosphorus alloys. J Appl Phys 41: 12-29.
4. Bernal JD (1960) Geometry of the structure of monatomic liquids. Nature 185: 68-70.
5. Lamparter P, Sperl W, Steeb S (1982) Atomic structure of amorphous metallic Ni81BI9. Z. Naturforschung 37:1223-1234.
6. Gaskell PH (1978) New structural model for transition metal-metalloid glasses. Nature 276: 484-485.
7. Frank FC (1952) Supercooling of Liquids. Proc Roy Soc Lond A 215: 43-46.
8. Inoue A, Arnberg L, Lehtinen B, Oguchi M, Masumoto T (1986) Compositional analysis of the icosahedral phase in rapidly quenched Al-Mn and Al-V alloys. Metallurgical and Materials Transactions A17: 1657-1664.
9. Yonezawa F, Nose S, Sakamoto S (1987) Computer study of glass transition. J. Non-Cryst. Solids 95: 83-93.
10. Sheng HW, Luo WK, Alamgir FM, Bai JM, Ma E (2006) Atomic packing and short-to-medium-range order in metallic glasses. Nature 439: 419-425.
11. Miracle DB (2004) A structural model for metallic glasses. Nat Mater 3: 697-702.
12. Ghafari M, Nakamura Y, Fukamichi K, Matsuura M (1994) Mössbauer study of amorphous Fe_2RE(RE=Ce, Er) alloys. Hyperfine Inter 83: 259-266.
13. Ghafari M, Keune W, Matsuura M, Schletz KP (1990) Hyperfine and x-ray investigations of amorphous Fe_2Er and Fe_2Ce alloys and the effect of hydrogenation on short-range order. Hyperfine Interactions 55: 947-951.
14. Margeat O, Respaud M, Amiens C, Lecante P, Chaudret B (2009) Ultrafine metallic Fe nanoparticles: synthesis, structure and magnetism. Beilstein J Nanotechnol 1: 108-118.
15. Day RK, Dunlop JB, Foley CP, Ghafari M, Pask H (1985) Preparation and Mössbauer study of a new Fe-rich amorphous alloy, $Fe_{90}Sc_{10}$. Solid State Communications 56: 843-845.
16. Ghafari M, Keune W, Brand RA, Day RK, Dunlop JB (1988) Local evidence for re-entrant magnetic behaviour in amorphous $Fe_{90}Zr_{10}$ alloys. Mater Sci Eng 99: 65- 68.
17. Ghafari M, Day RK, Dunlop JB, Mcgrath AC (1992) Spin coupling in amorphous $Fe_{90}Sc_{10}$ alloy. Journal of Magnetism & Magnetic Materials 104-107: 1668-1670.
18. Ghafari M, Kohara S, Hahn H, Gleiter H, Feng T, et al. (2012) Structural investigations of interfaces in $Fe_{90}Sc_{10}$ nanoglasses using high-energy x-ray diffraction. Appl Phys Lett 100: 133111-1-133111-4.
19. Sahoo B, Keune W, Schuster E, Sturhahn W, Toellener TS, et al. (2006) Amorphous Fe–Mg alloy thin films: magnetic properties and atomic vibrational dynamics. Hyperfine Inter 168: 1185-1190.
20. Ghafari M, Hahn H, Brand RA, Mattheis R, Yoda Y, et al. (2012) Structure of iron nanolayers embedded in amorphous alloys. Appl Phys Lett 100: 203108-1-4.
21. Fultz B, Ahn CC, Alp EE, Sturhahn W, Toellner TS (1997) Phonons in nanocrystalline ^{57}Fe. Physical Rev Lett, 79: 937-940.

22. Nguyen MC, Zhao X, Ji M, Wang CZ, Harmon B, et al. (2012) Atomic structure and magnetic properties of $Fe_{1-x}Co_x$ alloys. J Appl Phys 111: 07E338-1.

23. Mahalingam T, Raja M, Thanikaikarasan S, Sanjeeviraja C, Velumani S, et al. (2007) Electrochemical deposition and characterization of Ni-P alloy thin films. Mater Charact 58: 800-804.

24. Bera P, Seenivasan H, Rajam KS, Grips VKW (2012) Characterization of amorphous Co–P alloy coatings electrodeposited with pulse current using gluconate bath. Appl Surf Sci 258: 9544-9553.

25. Schlak T (2010) Beugungsexperimente an unterkühlten Metallschmelzen, Dissertation, Phys. Dept. Ruhr-University Bochum, Germany.